PERGAMON

International Journal of Multiphase Flow 28 (2002) 479–496

International Journal of Multiphase Flow

www.elsevier.com/locate/ijmulflow

Hydrodynamic force on spheres in cylindrical and prismatic enclosures

Zhi-Gang Feng, Efstathios E. Michaelides *

School of Engineering and Center for Bioenvironmental Research, Tulane University, New Orleans, LA 70118, USA

Received 20 February 2001; received in revised form 30 September 2001

Abstract

The Lattice–Boltzmann method (LBM) is used for the computation of the total hydrodynamic force acting on a solid sphere that settles in a viscous fluid contained in orthogonal cylindrical or prismatic enclosures. Creeping flow as well as flows with finite Reynolds numbers are computed. Among the several geometrical flow domains that are examined are: a sphere in an orthogonal circular cylinder and a sphere in a prismatic enclosure with various rectangular cross-sections. We also performed calculations on the flow and the hydrodynamic force developed on the sphere, when it does not move along the line of symmetry of the enclosure. In the last type of calculations, we have found out that a transverse component of the hydrodynamic force develops. In the absence of any rotation of the sphere and for the range of Reynolds numbers examined here, this force is directed towards the axis of symmetry of the enclosure.

1. Introduction

The problem of a particle settling within a three-dimensional enclosure is of particular importance in sedimentation processes, where particles fall freely inside confined spaces, in some chemical processes, where one or more particles move inside cylindrical or rectangular pipes and in mechanical processes, where plungers and pistons traverse confined spaces. The first researcher to consider this problem was Faxen (1922) who used the method of reflections for the movement of a sphere, under creeping flow conditions. Faxen was able to obtain an asymptotic solution for the total hydrodynamic force acting on a sphere, which is settling in an orthogonal circular

* Corresponding author. Tel.: +1-504-865-5764; fax: +1-504-862-8747.
E-mail address: emichael@tulane.edu (E.E. Michaelides).

0301-9322/02/$ - see front matter
PII: S0301-9322(01)00070-2

cylinder. When the trajectory of the center of the sphere is the centerline of the cylinder, Faxen's expression for the hydrodynamic force is given in terms of a "wall drag multiplier", K, as follows:

$$K_{\text{wall}} \equiv \frac{F_{\text{w}}}{6\pi a\mu U_0} = \frac{1}{1 - 2.015\lambda + 2.087\lambda^3}, \tag{1}$$

where λ is the ratio of the diameter of the sphere to that of the circular cylinder ($\lambda = d/D$), μ is the dynamic viscosity of the fluid, and U_0 is the settling velocity (which necessarily has to be low, because of the creeping flow assumption). The denominator in the first part of the expression is the Stokes drag force, for a solid sphere moving in an infinite fluid domain (always under creeping flow conditions). Therefore, the wall drag multiplier is the ratio of the actual drag experienced by the sphere in the enclosure divided by the drag on a sphere in an infinite fluid. It must be pointed out that Faxen's equation is valid only for small values of λ ($\lambda \leqslant 0.3$).

By using the same method of reflections Bohlin (1960) obtained a higher order approximation for the wall drag multiplier, which is as follows:

$$K_{\text{wall}} = \frac{1}{1 - 2.01443\lambda + 2.088777\lambda^3 - 6.94813\lambda^5 - 1.372\lambda^6 + 3.87\lambda^8 - 4.19\lambda^{10} + \cdots}. \tag{2}$$

At about the same time, Haberman and Sayre (1958) developed a theoretical method to compute K_{wall} for spheres settling in cylinders up to very high values of λ. Paine and Scherr (1975) used this method in order to compute this correction factor and tabulated their results for values of the diameter ratio in the range $0 \leqslant \lambda \leqslant 0.9$. A comparison between Eq. (2) and the exact theory by Haberman and Sayre (1958) shows that Eq. (2) yields accurate results up to $\lambda = 0.6$.

Apart form the analytical/computational studies, there are also several experimental studies pertaining to the settling of a sphere along the centerline of an orthogonal circular cylinder. Among them, the experimental results by Iwaoka and Ishii (1979), which show good agreement with the theoretical solution of Faxen and with Eq. (2).

An excellent exposition of the studies on the settling of spheres in enclosures may be found in the treatise by Happel and Brenner (1986), which devoted an entire chapter to discuss the wall effects on the motion of a single sphere. They considered creeping as well as inertia flow and stipulated that the total effect on the hydrodynamic force acting on the sphere is a simple linear combination of the separate effects of proximity to the outside boundary and inertia. Thus the total correction factor for the hydrodynamic force acting on a sphere is given by the expression:

$$K = K_{\text{wall}} + K_{\text{inertia}} - 1, \tag{3}$$

where K_{wall} is the wall effect at creeping flow as defined above and, K_{inertia} is the additional correction factor due to the inertia effects of the flow (higher Re). Eq. (3) simply implies that the drag on a sphere is composed of two additive terms: one term is due to the effect of the cylindrical boundary and the second due to the effects of the flow inertia. The latter is obtained from one of the empirical correlations for the drag coefficient, which are widely available in the literature. It must be pointed out that Eq. (3) is a semi-empirical equation, which emanates from the reduction of experimental data with λ in the range 0.1250–0.3125 and Reynolds numbers in the range 0.1–40. Despite its simplicity, the application of Eq. (3) yields significant errors, especially at higher values of the Reynolds numbers.

The reflection method, which was used in the case of the sphere settling in an orthogonal circular cylinder, cannot be employed in the case of multiple boundary problems, such as the problem of a sphere settling in a prism with a rectangular cross-section. Because of this, there are no known analytical results for the case of a sphere settling in a rectangular prism. However, the reflection method may be used in the case of a sphere moving between two infinite parallel plates. Faxen (1922) used this method in order to obtain an asymptotic analytical expression for K_{wall}, when the sphere moves very slowly (creeping flow) along the centerline between the two plane walls. His solution is as follows:

$$K_{\text{wall}} \equiv \frac{F_{\text{w}}}{6\pi a\mu U_0} = \frac{1}{1 - 1.004\lambda + 0.418\lambda^3 + 0.21\lambda^4 - 0.169\lambda^5 + \cdots}, \tag{4}$$

where λ is now defined as the ratio of the particle diameter and the perpendicular distance between the two plates ($\lambda = d/W$).

Among the experimental studies on prismatic enclosures, one must mention the one by Miyamura et al. (1981) who studied the settling of spheres in triangular and square prisms as well as between two parallel plates. In the case of the experiments conducted with the two parallel plates, they found in general a good agreement between their experimental data and Eq. (4) up to $\lambda = 0.4$.

It must be emphasized that all the above studies pertain to the sphere settling along the line of symmetry (centerline) of the enclosing shape. When the initial position of the sphere is off-center, the hydrodynamic force has a transverse component (lift force). This transverse force is a result of the inertia of the fluid and only becomes zero under Stokes (creeping) flow conditions for both solid and viscous spheres (Leal, 1992; Michaelides and Feng, 1995). Cherukat and McLaughlin (1994) conducted such a study at finite Reynolds numbers with one plane wall and calculated the transverse (lift) force on the sphere that settles in the proximity of a vertical plane.

In this study, we employ the Lattice–Boltzmann method (LBM) in three-dimensions in order to compute the total hydrodynamic force and the wall correction factors for a sphere settling in orthogonal cylinders and prisms with square and rectangular cross-sections. Comparisons of our numerical results with the results of known analytical and experimental studies show excellent agreement, a fact that validates the numerical method used. We determine the inertia effect of the particle motion by computing the hydrodynamic force at several values of the Reynolds number. We also use the LBM to compute the trajectories and the total hydrodynamic force (both lift and drag components) in the case of spheres that move off the lines of symmetry of orthogonal cylinders, prisms and parallel plates.

2. The LBM

The LBM is a relatively new method, developed for computational fluid mechanics. It is ideally suited for computations on particle–fluid interactions. The LBM originated from the lattice gas (LG) automata, a discrete particle kinetics method emanating from Boltzmann's kinetic theory of gases. The method utilizes a discrete lattice and discrete time. Frisch et al. (1986) are considered the first to apply this method to CFD and to have recovered a form of the Navier–Stokes equations from computations based on the LBM. Ladd (1994a,b) has done a great deal of

pioneering work for the simulation of fluid–particle interactions using the LBM. He provided a relationship between the exchange of momentum between the fluid and the solid boundary nodes. In his method, it is assumed that the fluid particles also occupy the volume of the solid particles. Aidun et al. (1998) made some modifications that decompose the force on the solid particles into a body force and a hydrodynamic force exerted on the surface. They did not assume that the fluid particles fill the same space as the solid particles. Behrend (1995) discussed the various treatments on the solid to fluid boundary including treating the solid–fluid nteractions on the links between the lattice nodes rather than on the lattice nodes themselves as Ladd proposed. It has been observed that, despite all these modifications, most researchers who apply the LBM prefer to use the original approach by Ladd (1994a,b). We have also found that for our applications with solid spheres and irregular particles, the approach by Ladd is the most efficient and provides excellent results. An excellent review on the subject has been conducted by Chen and Doolen (1998).

In the LBM, the flow domain is divided into a discrete lattice, which spans the whole computational domain. A distribution function, $f(\boldsymbol{x},t)$, for the density of the fluid in the lattice node is used to represent the flow of a real fluid. The Lattice–Boltzmann equation for the distribution function is given by the following expression:

$$f_i(\boldsymbol{x}+\boldsymbol{e}_i,t+1)-f_i(\boldsymbol{x},t)=-\frac{1}{\tau}\left[f_i(\boldsymbol{x},t)-f_i^0(\boldsymbol{x},t)\right], \tag{5}$$

where $f(\boldsymbol{x},t)$ is the fluid–particle distribution function, $f^0(\boldsymbol{x},t)$ is the equilibrium distribution function, τ is the relaxation time, and t is the lattice simulation time. The subscript, i, represents the several directions, towards which the particle may move.

The present study is three-dimensional and we use a so-called "3d15" bit LBM model. According to this model, a given lattice point may move in 15 directions towards its neighboring lattice points. When this lattice point is considered as the center of a cube, 14 of these directions are towards the centers of the six cubic faces and towards the eight vertices of the cube. The 15th direction corresponds to the zero (null) vector, in which case the lattice point does not move. All the 15 velocity directions $\boldsymbol{e}_i$ $(i=0,1,2,\ldots,14)$ are shown in Fig. 1, with $i=0$ corresponding to the zero vector.

In an explicit way, all these vectors $\boldsymbol{e}_i$ $(i=0,1,2,\ldots,14)$ correspond to the column vectors of the following matrix:

$$\boldsymbol{E}=\begin{bmatrix} 0 & 1 & -1 & 0 & 0 & 0 & 0 & 1 & -1 & 1 & -1 & 1 & -1 & 1 & -1 \\ 0 & 0 & 0 & 1 & -1 & 0 & 0 & 1 & -1 & 1 & -1 & -1 & 1 & -1 & 1 \\ 0 & 0 & 0 & 0 & 0 & 1 & -1 & 1 & -1 & -1 & 1 & 1 & -1 & -1 & 1 \end{bmatrix}. \tag{6}$$

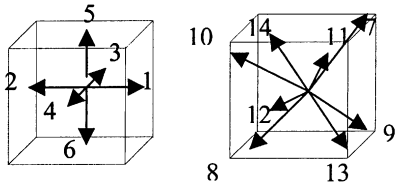

Fig. 1. Velocity vectors for a 3d15 LBM model.

At each node of the lattice, the density and momentum can be written in terms of the distribution function $f(\boldsymbol{x},t)$ as follows:

$$\rho(\boldsymbol{x},t)=\sum_i f_i(\boldsymbol{x},t), \tag{7}$$

and

$$\rho(\boldsymbol{x},t)\vec{\boldsymbol{u}}=\sum_i f_i(\boldsymbol{x},t)\boldsymbol{e}_i. \tag{8}$$

Since the lattice formed in this problem has a density and a momentum function, one may obtain its characteristics as a mass of a viscous fluid, which necessarily obeys the Navier–Stokes equations. The viscosity of this fluid would be related to the response time of the interactions of the lattice points. For the computations that follow, it is sufficient to consider a single relaxation (response) time, τ, for these interactions. Given the dimensions of the lattice, the relaxation time τ yields the kinematic viscosity of the fluid as follows (Ladd, 1994a):

$$v=(2\tau-1)/6. \tag{9}$$

We define the expression for the equilibrium distribution function of the lattice points, $f^0(\boldsymbol{x},t)$, as:

$$f_i^0(x,t)=A_i+B_i(e_i\cdot u)+C_i(e_i\cdot u)^2+D_i(u\cdot u), \tag{10}$$

where, A_i, B_i, C_i and D_i are constants, derived by the constraints of the constituent (closure) equations. Because we wish to model flows with finite Reynolds numbers, we adopt the following values for the 60 model constants that are needed for the calculations:

$$A_0=\frac{1}{8}\rho,\quad B_0=C_0=0,\quad D_0=-\frac{1}{3}\rho, \tag{11}$$

$$A_i=\frac{1}{8}\rho,\quad B_i=\frac{1}{3}\rho,\quad C_i=\frac{1}{2}\rho,\quad D_i=-\frac{1}{6}\rho\ \ (i=1,2,\ldots,6), \tag{12}$$

$$A_i=\frac{1}{64}\rho,\quad B_i=\frac{1}{24}\rho,\quad C_i=\frac{1}{16}\rho,\quad D_i=-\frac{1}{48}\rho\ \ (i=7,8,\ldots,14). \tag{13}$$

Under this formulation, in order to simulate a zero-*Re* (Stokes flow) one may simply set $C_i=D_i=0$ $(i=0,1,2,\ldots,14)$.

In order to simulate the hydrodynamic interactions between the solid particles in a suspension flow, the LBM must be modified to incorporate the boundary conditions imposed on the fluid by the solid particles. The surface of the boundary cuts some of the links between the lattice nodes, and the fluid particles moving along these links interact with the solid surface at boundary nodes, which are placed halfway along the links. In this case the boundary node, $\boldsymbol{r}_b$, is defined as the middle of the link. Such boundary nodes approximate the surface of the particles. Obviously, in order to have a more precise representation of the shape of a particle, a higher number of lattice units are needed (bigger particle in comparison to the computational domain). The required no-slip boundary condition on the surface of the moving particles is achieved by the requirement that the fluid velocity has the same value at the boundary nodes as the particle velocity, $\boldsymbol{u}_b$. Thus, the particle velocity at a boundary node may be written explicitly as follows:

$$\boldsymbol{u}_{\mathrm{b}} = \boldsymbol{U} + \boldsymbol{W}_{\mathrm{b}} \times (\boldsymbol{x} - \boldsymbol{R}), \tag{14}$$

where $\boldsymbol{U}$ is the particle translational velocity, $\boldsymbol{W}_{\mathrm{b}}$ is the particle rotational velocity, and $\boldsymbol{R}$ is the position of the center of the particle. To account for the momentum exchange change when $\boldsymbol{u}_{\mathrm{b}}$ is not zero, a collision function is used, which is given by the following expression:

$$f_{i'}(\boldsymbol{x}, t^{+} + 1) = f_i(\boldsymbol{x}, t^{+}) - 2B_i(e_i \cdot U_{\mathrm{b}}), \tag{15}$$

where $\boldsymbol{x}$ is the position of the node adjacent to the solid-surface with velocity $\boldsymbol{U}_{\mathrm{b}}$, t^{+} is the post-collision time, which is taken the same as in Ladd (1994a) and i' denotes the direction, which is opposite to the incident direction, i (reflection). More details on this part of the method may be found in Ladd (1994a,b).

Therefore, the hydrodynamic force exerted on the solid particle at the boundary node is

$$\boldsymbol{F}\left(\boldsymbol{x} + \frac{1}{2}\boldsymbol{e}_i, t\right) = 2\boldsymbol{e}_i[f_i(\boldsymbol{x}, t^{+}) - 2B_i(\boldsymbol{U}_{\mathrm{b}} \cdot \boldsymbol{e}_i)]. \tag{16}$$

It must be pointed out that momentum is exchanged locally between the fluid and the solid particle, but the combined momentum of the solid and the fluid is conserved globally. The total force $\boldsymbol{F}_{\mathrm{t}}$ and the torque $\boldsymbol{T}_{\mathrm{t}}$ on the solid particle can be obtained by summing up all the forces and torques acting on this particle:

$$\begin{aligned} \boldsymbol{F}_{\mathrm{t}} &= \sum_i \boldsymbol{F}\left(\boldsymbol{x} + \frac{1}{2}\boldsymbol{e}_i\right), \\ \boldsymbol{T}_{\mathrm{t}} &= \sum_i \left(\boldsymbol{x} + \frac{1}{2}\boldsymbol{e}_i\right) \times \boldsymbol{F}\left(\boldsymbol{x} + \frac{1}{2}\boldsymbol{e}_i\right). \end{aligned} \tag{17}$$

In the numerical scheme, which is adopted for the solution of the resulting set of equations, both the translational and rotational velocities are updated at each time step by using the following formulae:

$$\boldsymbol{U}_0(t+1) = \boldsymbol{U}_0(t-1) + 2M^{-1}\boldsymbol{F}(t) \tag{18}$$

and

$$W(t+1) = W(t-1) + 2\boldsymbol{I}^{-1} \cdot \boldsymbol{T}(t), \tag{19}$$

where M and $\boldsymbol{I}$ are the mass (scalar) and inertia (vector) of the particle.

3. Simulation of particle motion in an orthogonal cylinder

The three-dimensional LBM is first used to compute the drag force on a spherical particle settling in a cylinder. Since the particle is moving relative to the boundary, an exact simulation of the system with a fixed set of coordinates requires constantly updating the computational domain or using a very long cylinder in the computational domain to account for the entrance length, until the sphere reaches its terminal velocity. Instead of this, we have used a coordinate system fixed on the sphere. Hence, the problem becomes equivalent to that of a cylinder full of fluid with unidirectional velocity U_0 passing over a stationary sphere. The boundary condition at the surface

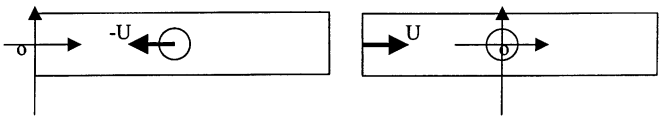

Fig. 2. Schematic diagram of a particle settling in a cylinder.

of the cylinder becomes one of constant unidirectional velocity, U_0. This situation is depicted in the schematic diagram of Fig. 2. Under these conditions, gravity acts from the right to the left of the figure. The calculated steady-state hydrodynamic forces on the sphere in the two configurations depicted in the figure are identical.

The 3d15 bit LBM is used in all the simulations. The diameter of the sphere is always kept equal to at least 18 lattice units or larger. We have found from size validation studies that this minimum size for the sphere yields results, which are accurate to 1.0%. The moving boundary conditions on the surface are applied using the "bounce and back rule" (Ladd, 1994b). The outlet boundary condition in the computational domain is set to be stress free ($du/dx = 0$). Hence, we derived for the discrete lattice points the condition $u[nx] = u[nx - 1]$. Furthermore, by using the mass and momentum conservation equations (7) and (8), we are able to solve for the unknown fluid density at the outlet boundary, and subsequently apply the domain marching rules.

4. Results and discussions

4.1. A solid sphere in a circular cylinder

The problem of a solid sphere settling axially in a circular cylinder has been well-studied, both analytically and experimentally. In this study we are deriving the results of this problem in order to validate the numerical scheme we are using in the LBM. Numerical grids with sizes from $50 \times 50 \times 200$ to $90 \times 90 \times 300$ were used in the computations of the total hydrodynamic force (and, hence, of the wall drag multiplier) depending the diameter ratio of the sphere and the cylinder. The minimum inlet length is about three times the sphere diameter upstream of the sphere and the minimum outlet length is about seven times the diameter of the sphere downstream. Parametric studies on these dimensions have shown that these inlet and outlet dimensions are sufficient for the establishment of steady-state conditions at all conditions examined here.

We have compared our results for the drag wall multiplier with the results derived by the analytical method of Haberman and Sayre (1958) as computed and tabulated by Paine and Scherr (1975). Table 1 shows this comparison of the wall drag multipliers.

It is apparent that there is a very good agreement between the numerical and the analytical results, especially at the lower values of λ. Our numerical calculations also show that the

Table 1
Comparison of previous solutions and present numerical results

$\lambda(= d/D)$	0.2	0.3	0.4	0.5	0.6	0.7	0.8
K (present)	1.70	2.41	3.68	6.18	11.92	26.88	85.03
K (analytical)	1.68	2.37	3.60	5.96	11.16	25.01	78.52

computational results at high values of λ can be improved by the use of a finer grid in the fluid gap between the sphere and the enclosure.

Another comparison of the present computational method was accomplished at very low Reynolds numbers ($0.1 < Re < 4.0$). Fig. 3 shows a comparison between the analytical solution at Stokes flow, the present LBM results, and a set of experimental data at low Reynolds numbers (Jourdan, 2000). It is obvious that there is very good agreement with all sets of data, a fact that further validates the numerical scheme used in this work.

By using the LBM in the solution of the problem of a sphere settling in a cylinder, we were able to compute the wall correction factors for Stokes flow as well as for inertia flows. We have found out from our computations that, when the diameter ratio, λ, is greater than 0.5 the inertia effect is insignificant compared to the wall effect, for Reynolds numbers up to 20. At values of λ, less than 0.5 one has to account for the inertia effect on the correction factor. We have also found out that, with the grid size and the type of simulation box we chose, the LBM fails to converge for $Re > 50$. However, we believe by using a more refined grid, one is able to compute results at higher values of Re (in this case, the computational time would increase significantly).

Table 2 shows the wall correction factors at different Reynolds numbers. By comparing the results at finite Re with those of the Stokes solution, we are able to determine the effect of the flow inertia on the wall multiplier. It is evident from the results of Table 2 that for $\lambda = 0.8$ and $0 < Re \leqslant 20$, the inertia effect amounts to less than 5% of the total value of the correction factor. The corresponding figure at $\lambda = 0.6$ is about 7%, while at $\lambda = 0.4$ the inertia accounts for more than 14% of the value of the correction factor. This indicates that the effect of inertia on the wall correction factor is very low at high values of the parameter λ. The semi-empirical data, calculated by using Eqs. (2) and (3) with Rowe's expression (Clift et al., 1978; Michaelides, 1997) for the drag

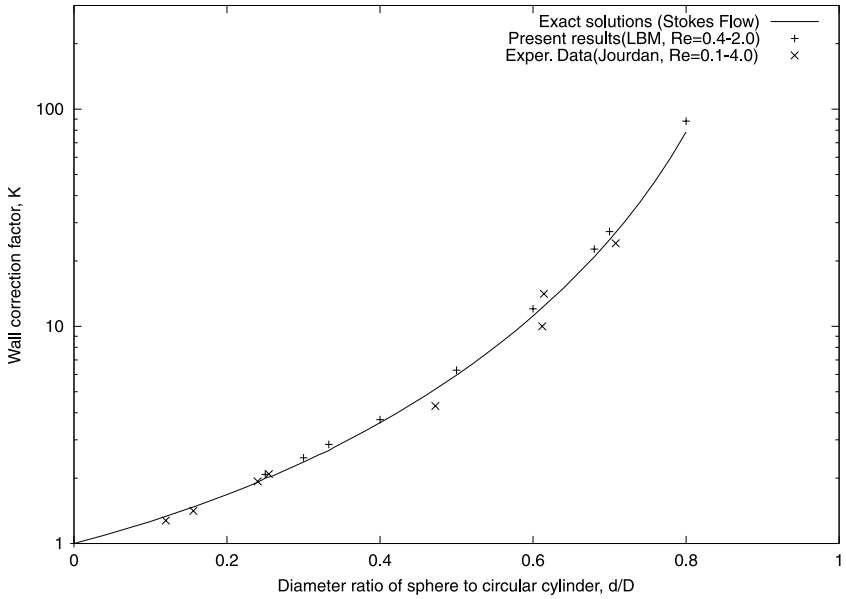

Fig. 3. Wall correction factors for single solid spheres in a circular cylinder.

Table 2
Wall correction factors at different Reynolds numbers

		λ		
		0.4	0.6	0.8
Stokes flow	Exact solution	3.60	11.86	78.52
	Present method	3.68	11.92	85.03
$Re = 10$	Present method	3.82	12.30	86.23
	Semi-empirical	4.37	11.93	79.29
$Re = 20$	Present method	4.21	12.73	88.88
	Semi-empirical	4.83	12.39	79.75

coefficient at higher Re, are also shown in the table. Rowe's expression for the drag coefficient has been used in this study for the drag coefficient of a sphere in an infinite fluid domain, because it is the most frequently used expression in particle flow simulations and it agrees well with experiments in the pertinent range of Reynolds numbers used in this study. This expression is as follows:

$$C_{\text{inertia}} = \frac{24}{Re}\left(1 + 0.15Re^{0.687}\right). \tag{20}$$

A glance at Table 2 shows that there is a small discrepancy between the semi-empirical data and the numerical results obtained by this method. This discrepancy is more pronounced at lower values of λ (at $Re = 20$, it is about 15% at $\lambda = 0.4$, but only 10% at $\lambda = 0.8$). The discrepancy is most probably due to the fact that the two effects of inertia and of the flow confinement (wall) may not be always linearly combined as Eq. (3) implies.

4.2. A solid sphere in a rectangular prism

In this section, we apply the LBM to compute the wall and inertia effects on a single rigid sphere settling in several orthogonal prisms of rectangular cross-sections. Fig. 4 shows the system and the computed flow velocity field in a rectangular prism with cross-sectional length to width ratio equal to 2.0 ($L/W = 2$) and sphere diameter to width ratio $\lambda = d/W = 0.5$. In this case, we have used $200 \times 40 \times 80$ lattice units with the diameter of the sphere being equal to 20 lattice points. The direction of the gravity in Fig. 4 is in the $-x$ direction.

From the outset it must be pointed out that the case of the single-phase fluid flow in a rectangular prism is different than that of the flow in a cylinder, because of the secondary flow, which are developed in a direction perpendicular to the main component of the velocity. This secondary flow is caused by the corners of the prism and is developed in all types of polygonal prisms. This phenomenon is well known in the fluid dynamics literature and does not need further elaboration (Schlichting, 1978). In the case of the flow induced by a falling sphere, one expects to encounter a similar type of secondary flow, which would develop in the horizontal plane (that is a plane perpendicular to the direction of gravity) near the corners of the prism. For this reason we have calculated the secondary flow developed in the horizontal plane through the center of the sphere, for a sphere settling in orthogonal cylindrical and a square prism. The conditions for the computations are: $Re = 0.48$ and $\lambda = 0.4$. We have plotted the results of the computations on a

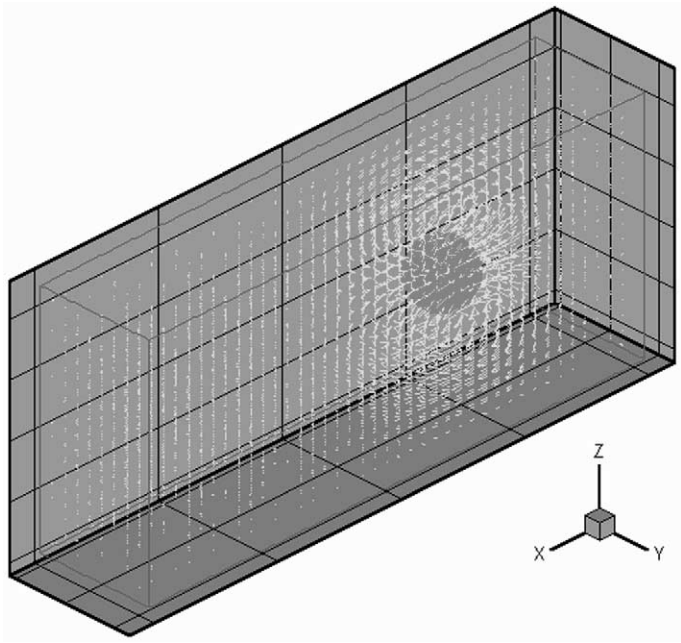

Fig. 4. A solid sphere in a square cylinder with $d/W = 0.5$.

horizontal plane that passes through the center of the sphere in Fig. 5. It is obvious that the secondary flow patterns created in the two horizontal planes are markedly different. This implies that there will be significant differences in the magnitude of the hydrodynamic force exerted on the sphere. Regarding the last figure, it must be pointed out that the magnitude of the velocity in Fig. 5 is approximately two orders below the magnitude of the settling velocity of the sphere for both the cylinder and for the square prism.

For the case of a sphere settling in a rectangular prism, there are no analytical solutions available. The work by Faxen (1922), covers the case of a sphere settling at creeping flow conditions between two infinite parallel plates, which is essentially the case of a sphere settling in a

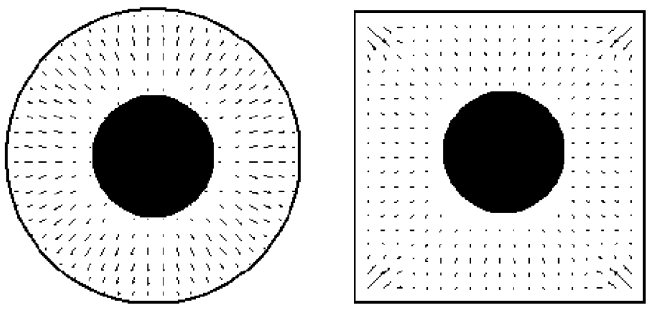

Fig. 5. Secondary flow created in a cylinder and a square prism.

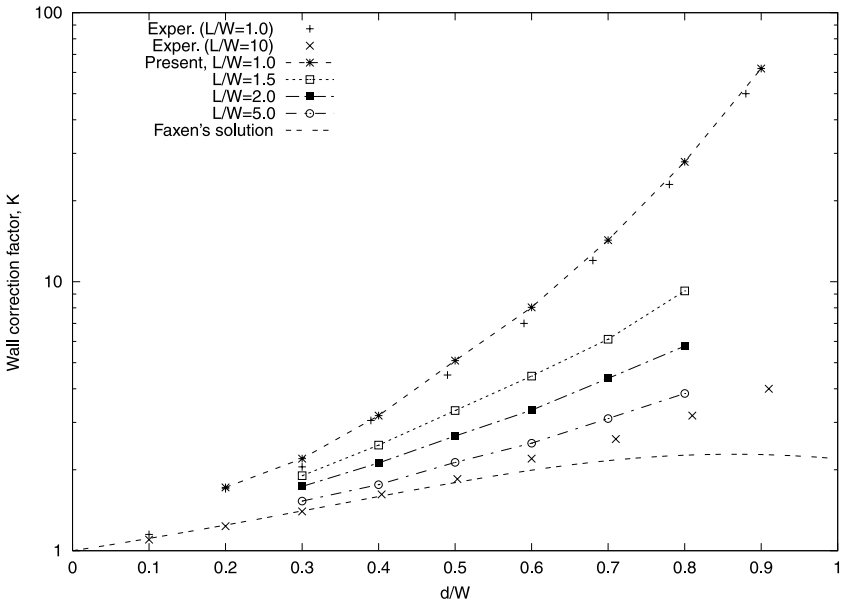

Fig. 6. Wall correction factors for various rectangular cylinders.

rectangular prism of infinite length to width ratio. The final result of this study is the asymptotic equation (4).

Fig. 6 shows the computed wall correction factors with various rectangular shapes. The experimental data shown are from the study of Miyamura et al. (1981) who presented the wall correction factors for two ratios of the parameter L/W, namely 1 and 10. Faxen's asymptotic solution for the two parallel plates is also plotted in the same figure. It is apparent that this solution is valid up to $\lambda = 0.5$.

Table 3 shows the detailed results for the correction factors obtained by the LBM for various orthogonal rectangular prisms and for several values of the parameters d/W and L/W. The same

Table 3
Wall correction factors for various orthogonal rectangular prisms

$L/W = 1.0$								
$\lambda(= d/W)$	0.2	0.3	0.4	0.5	0.6	0.7	0.8	0.9
K	1.72	2.30	3.18	5.01	8.03	13.98	27.9	61.8
$L/W = 1.5$								
$\lambda(= d/W)$	0.3	0.4	0.5	0.6	0.7	0.8		
K	1.90	2.47	3.32	4.46	6.11	9.24		
$L/W = 2.0$								
$\lambda(= d/W)$	0.3	0.4	0.5	0.6	0.7	0.8		
K	1.73	2.12	2.67	3.33	4.37	5.76		
$L/W = 5.0$								
$\lambda(= d/W)$	0.3	0.4	0.5	0.6	0.7	0.8		
K	1.53	1.75	2.11	2.48	3.06	3.78		

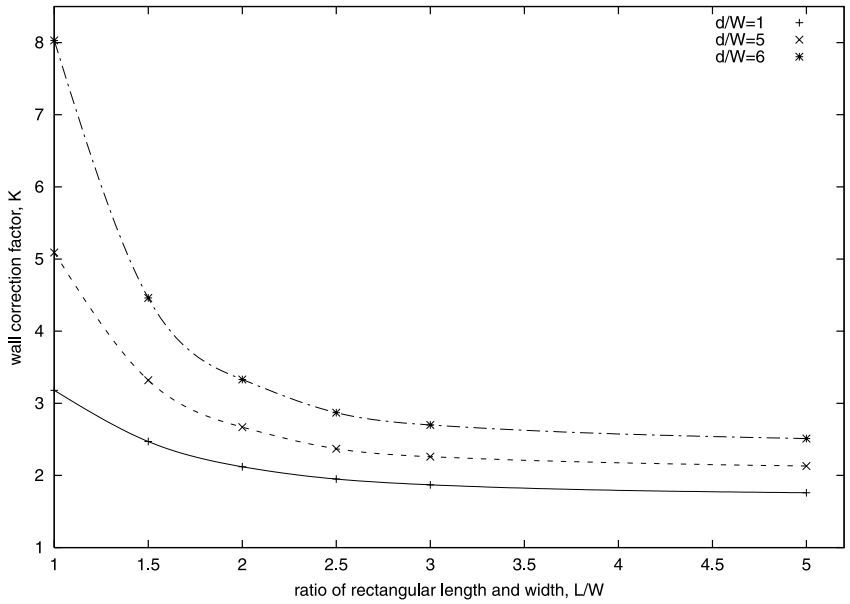

Fig. 7. Wall correction factors vs rectangular shape.

data are also plotted in Fig. 7. The value $L/W = 1$ represents the case of an orthogonal square prism. The case of two parallel plates would correspond to the value $L/W \to \infty$. It is evident, from Table 3, that our numerical results agree very well with the experimental data of Miyamura et al. (1981) for the case of an orthogonal square prism ($L/W = 1$). The results also show (this is clearer in Fig. 7) that the effect of the parameter L/W on the correction factors is very significant in the range $1 < L/W < 3$ and that this effect diminishes considerably for values $L/W > 3$. It must be pointed out, however, that this effect is not negligible, as demonstrated in Fig. 6 by the considerable difference, which is apparent between the curves for $L/W = 5$ and the experimental data for $L/W = 10$. Table 3 and Figs. 6 and 7 show that, while the parameter d/W is the most significant factor for the wall correction factors, the distance of the other side boundaries (that is the parameter L/W) still plays a significant role in the determination of the total correction factor.

The velocity fields in two vertical cross-sections of the orthogonal prism with $L/W = 2.0$ are also shown in Fig. 8. These vertical sections are through the center of the sphere, in the x–z and the x–y planes (gravity acts in the $-x$ direction). It is observed that the velocity disturbance is essentially confined in the immediate vicinity of the sphere, with very low-level disturbances at distances further than one diameter.

4.3. Off-center settling of a solid sphere in a cylinder or a rectangular prism

The problems of a single solid sphere settling off the cylinder centerline or off the center plane of two parallel plates have also been discussed by Happel and Brenner (1986) for the case of creeping flow. However, it is well known (Leal, 1992; Michaelides, 1997) that any solutions under the Stokes flow assumption (creeping flow) yields a hydrodynamic force, which is in the direction of

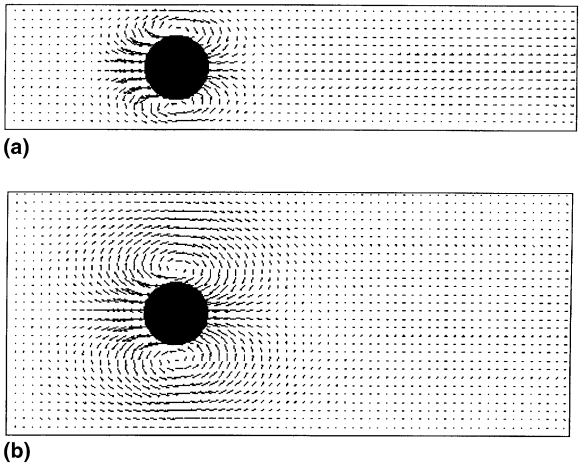

Fig. 8. Velocity fields around a solid sphere with $L/W = 2.0$: (a) cross-section at $y = L/2$; (b) cross-section at $z = W/2$.

the flow (drag force only with zero lift). The transverse component of the hydrodynamic force (lift), which acts laterally and determines the true trajectory of the sphere, only appears in flows with inertia. Feng et al. (1994) using direct numerical simulations examined numerically this problem in two-dimensions (cylinder between two infinite plates) and showed that, when the two-dimensional particle is off-center, there is always a transverse component of the hydrodynamic force, always acting towards the center. This, combined with the viscosity of the fluid, results in damped oscillations around the centerline and in the particle's finally settling along the centerline of the channel. Feng et al. (1994) also found that when the Reynolds number is very small but finite and the channel is wide, the particle will simply approach slowly the centerline and then will settle along this line. However, for higher Reynolds numbers (in this case $Re = 3.2$) the sphere would overshoot the centerline and would describe damped oscillations around it.

In this section, we consider the case of a single solid sphere in narrow circular cylinders with diameter ratio $\lambda = d/D = 2/3$. The initial position of the center of the sphere is at a distance $y = 0.1D$ off the cylinder's axis of symmetry. In this case, we have achieved flows of different Reynolds numbers (defined with respect to the equilibrium terminal velocity) by varying the fluid to particle density ratio. Thus, we were able to achieve values of Re in the range 4.0–11.3.

Fig. 9 shows the two components of the total hydrodynamic force for this flow situation, separated as longitudinal and transverse forces. It is observed that the longitudinal component (drag force) reaches rather quickly its equilibrium value. The behavior of the transverse component of the force depends on the value of Reynolds number: at the low value of Re, (4.0) the transverse component of the force starts with a very low magnitude, reaches its equilibrium value (0.0) rather quickly and remains at approximately this value. However, at higher values of Re (7.8 and 11.3), the initial value of the transverse component is higher. As the sphere approaches the center and then overshoots it, the sign of this component changes and this results in damped oscillations around the centerline. Finally, the transverse force approaches asymptotically the value zero.

Fig. 10 shows the trajectories described by the spheres under the three values of the Reynolds numbers mentioned above. It is apparent that the magnitude of the oscillations around the

centerline increases with the value of *Re*. There is a qualitative agreement of these results with those of the two-dimensional cases examined by Feng et al. (1994). However, we have found that, in the three-dimensional case, under the same ratio of d/D, the damped oscillations around the

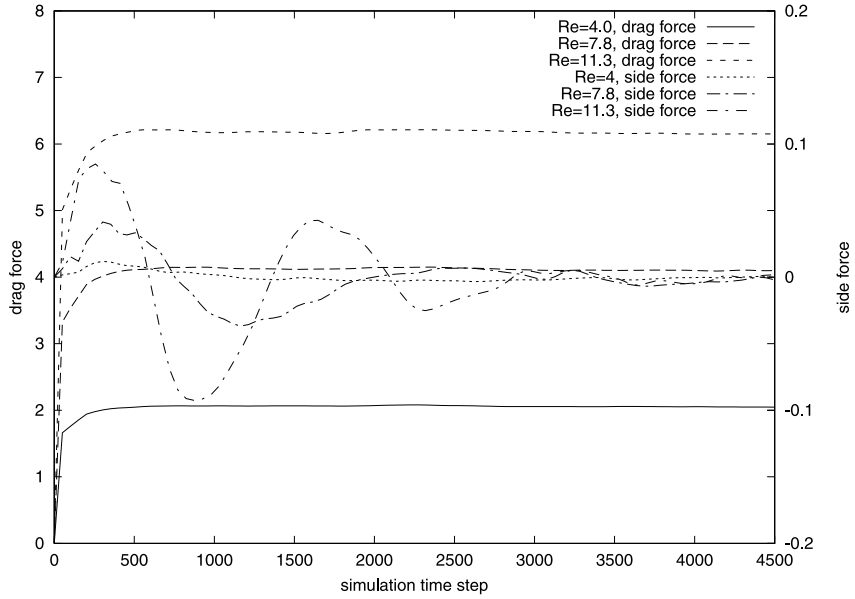

Fig. 9. The drag force and side force on the sphere settling off the centerline in a circular cylinder.

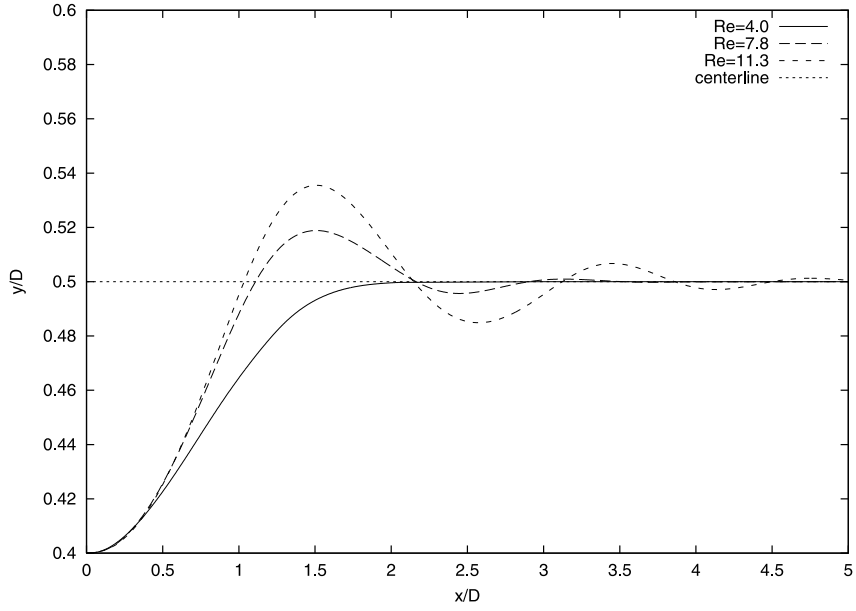

Fig. 10. Settling trajectory of a solid sphere in a circular cylinder at different Reynolds numbers.

centerline start at higher values of the Reynolds number, which signify that the complete (three-dimensional) enclosure of the fluid around the sphere has a stabilizing effect on its trajectory.

We have also simulated the settling motion of a solid sphere, starting in an off-center position in the case of a square rectangular prism at various values of the Reynolds number in the range $4.96 < Re < 34.8$ and for a diameter to side ratio d/L equal to 2/3. The trajectories of the sphere in all of these cases are shown in Fig. 11. Two observations can be made by comparing the results in Figs. 10 and 11: first, that the oscillations of the sphere around the center of the square prism start at higher values of Re (than in the case of the cylinders) and second, that the magnitude of the oscillations is lower for comparable values of Re. Both these observations lead us to the conclusion that the more confined space in the circular geometry generates a stronger lateral force on the sphere. This phenomenon is better observed in the results depicted in Fig. 12, where a comparison is made of the trajectories of the sphere inside the circular cylinder and inside the square prism (the ratio of the dimensions of the sphere to that of the enclosing solid is equal to 2/3 in all cases). It is apparent that, at similar Reynolds numbers, the lateral force in the case of the circular cylinder is stronger.

All our simulations, which are at $Re < 35$ and in the absence of any initial rotation imposed on the particle, showed that the transverse force is directed towards the axis of symmetry of the enclosure. Even if the sphere started its motion with an initial finite value of the angular velocity, at the range of the Reynolds numbers examined here, the angular velocity of the sphere will be quickly damped to reach the value of zero and the sphere will find its equilibrium position at the axis of symmetry, independent of the initial position and angular velocity. This is in agreement with the computations by Zhu (2000) who observed that, for Re "less than around 30", a particle would migrate towards the axis of symmetry, even when it is rotating at the inception of its

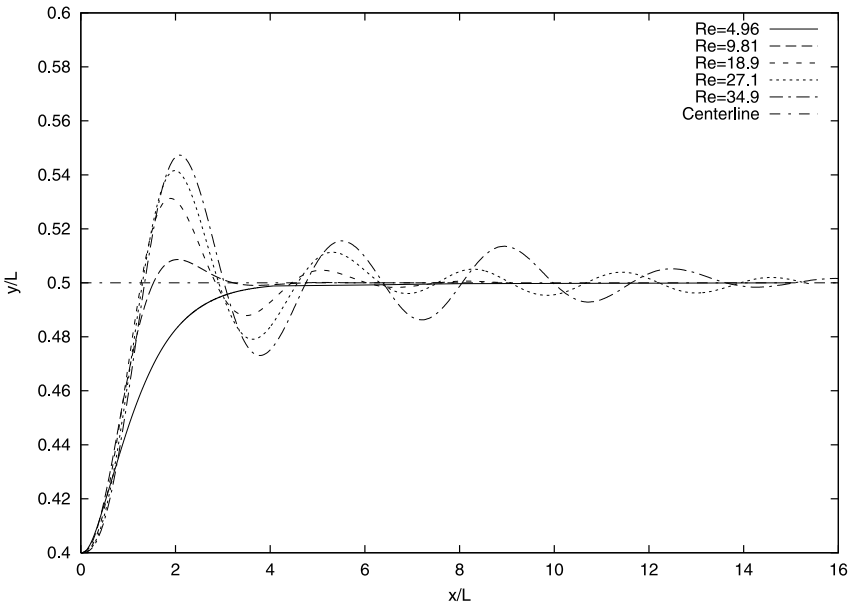

Fig. 11. Trajectory of a solid sphere in a square cylinder, starting at an off-center position.

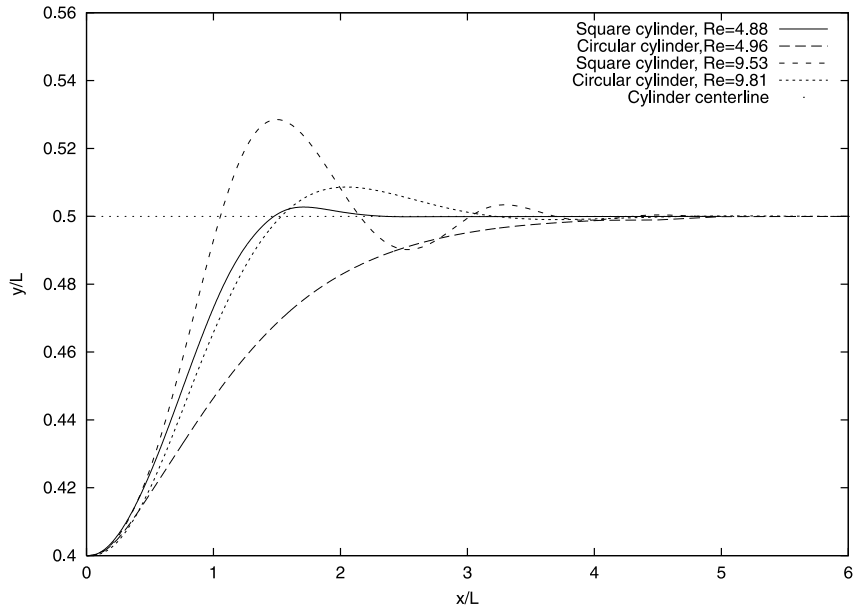

Fig. 12. Comparison of trajectories for a particle settling in a square cylinder and circular cylinder.

motion. Zhu's computations also showed that at higher values of Re and with an initial rotation, there is an equilibrium position for the sphere, outside the axis of symmetry, which is dictated by its initial position and the initial angular velocity. Finally, at higher values of Re ($Re > 100$) it is well known that the wake formed at the back of the sphere would influence its position in a periodic way, a fact that is also in agreement with the computations by Zhu (2000).

5. Conclusions

The three-dimensional LBM has been used to compute the total hydrodynamic force and the wall correction factors for solid spheres settling in orthogonal cylindrical and prismatic enclosures. The numerical results were validated by comparing the case of a sphere settling in a cylinder with available analytical and experimental data. The results show that the effects of inertia and proximity to a wall are not simply to be added. It was also found in the case of cylindrical enclosures that, when the diameter ratio, λ, is greater than 0.5, the inertia effect is insignificant compared to the wall effect, up to $Re = 20$. At lower values of the diameter ratio one has to account for the inertia effect on the correction factor. In the case of the rectangular prisms, the results also show that the effect of the length to width ratio on the correction factors is very significant in the range $1 < L/W < 3$ and that this effect diminishes considerably for values $L/W > 3$, without becoming negligible. When the sphere is released from an off-center position, the hydrodynamic force has a transverse (lift) as well as a longitudinal (drag) component. In this case, the longitudinal component reaches rather quickly its equilibrium value. The transverse component is slower to reach its equilibrium value (which is zero). At the low value of Re (4.0),

the transverse component of the force starts with a very low value, reaches its equilibrium value and remains at approximately this value. At higher values of *Re* (7.8 and 11.3), the starting value of the transverse component is higher and this component exhibits damped oscillations, but its direction is always towards the axis of symmetry of the enclosure. The trajectory of the sphere in this case is oscillatory too. By comparing the two-dimensional with the three-dimensional results, we have found that in the three-dimensional case, under the same ratio of d/D, the damped oscillations around the centerline start at higher values of the Reynolds number. This signifies that the complete (three-dimensional) enclosure of the fluid around the sphere has a stabilizing effect on its trajectory. Regarding the oscillations of the sphere in cylinders versus prisms with the same dimensional parameters, we have found that the damped oscillations of the sphere around the center of the square prism start at higher values of *Re* and, that the magnitude of the oscillations is lower for comparable values of *Re*. Both of these observations lead us to the conclusion that the damping on the transverse motion of the sphere is higher in the case of the square prism.

Acknowledgements

This work was partly supported by grants from the ONR to the Tulane/Xavier Center for Bioenvironmental Research as well as by a grant from the NASA/EPSCoR program to Tulane University. The authors are thankful for this support.

References

Aidun, C.K., Lu, Y.-N., Ding, E.-J., 1998. Direct analysis of particulate suspensions with inertia using the discrete Boltzmann equation. J. Fluid Mech. 373, 287.

Behrend, O., 1995. Solid–fluid boundary in particle suspension simulations via the lattice Boltzmann method. Phys. Rev. E 52, 1164–1165.

Bohlin, T., 1960. Terminal velocities of solid spheres in cylindrical enclosures. Trans. R. Inst. Technol. (Stockholm), No. 155.

Chen, S., Doolen, G.D., 1998. Lattice Boltzmann method for fluid flows. Annu. Rev. Fluid Mech 30, 329–364.

Cherukat, P., McLaughlin, J.B., 1994. The inertial lift on a rigid sphere in a linear shear flow field near a wall. J. Fluid Mech. 263, 1.

Clift, R., Grace, J.R., Weber, M.E., 1978. Bubbles, Drops and Particles. Academic Press, New York.

Faxen, H., 1922. Resistance to the movement of a rigid sphere in a viscous fluid bounded by two parallel flat walls. Ann. Phys. 68, 89–119.

Feng, J., Hu, H.H., Joseph, D.D., 1994. Direct simulation of initial value problems for the motion of solid bodies in a Newtonian fluid. Part 1. Sedimentation. J. Fluid Mech. 95, 95–134.

Frisch, U., Hasslacher, Romeau, Y., 1986. Lattice-gas automata for the Navier–Stokes equations. Phys. Rev. Lett. 56, 1505–1508.

Haberman, W.L., Sayre, R.M., 1958. Motion of rigid and fluid spheres in stationary and moving liquids inside cylindrical tubes. David Taylor Model Basin, Report No. 1143, US Navy, Washington DC.

Happel, J., Brenner, H., 1986. In: Low Reynolds Number Hydrodynamics. Martinus Nijhoff, Dordrecht (reprint of the 1963 edition).

Iwaoka, M., Ishii, T., 1979. Experimental wall correction factors of single solid spheres in circular cylinders. J. Chem. Eng. Jpn. 12, 239–242.

Jordan, S., 2000. Particle sedimentation in cylindrical tubes. DEA report, Universite Claude Bernard, Lyon, France.

Ladd, A.J.C., 1994a. Numerical simulations of particulate suspensions via a discretized Boltzmann equation. Part 1. Theoretical foundation. J. Fluid Mech. 271, 209–285.

Ladd, A.J.C., 1994b. Numerical simulations of particulate suspensions via a discretized Boltzmann equation. Part 2. Numerical results. J. Fluid Mech. 271, 209–285.

Leal, L.G., 1992. In: Laminar Flow and Convective Transport Processes. Butterworth-Heineman, Boston.

Michaelides, E., 1997. Review – The transient equation of motion for particles, bubbles, and droplets. J. Fluids Eng. 119, 233–247.

Michaelides, E.E., Feng, Z.-G., 1995. The equation of motion of a small viscous sphere in an unsteady flow with interface slip. Int. J. Multiphase Flow 21, 315–321.

Miyamura, A., Iwasaki, S., Ishii, T., 1981. Experimental wall correction factors of single solid spheres in triangular and square cylinders, and parallel plates. Int. J. Multiphase Flow 7, 41–46.

Paine, P.L., Scherr, P., 1975. Drag coefficients for the movement of rigid spheres through liquid-filled cylindrical pores. Biophys. J. 15, 1087–1091.

Schlichting, H., 1978. Boundary Layer Theory. McGraw Hill, New York.

Zhu, M., 2000, Direct numerical simulation of solid–liquid flow of Newtonian and viscoelastic fluids. Ph.D. dissertation, Department of Mechanical Engineering and Applied Mechanics, University of Pennsylvania.